Three-body calculations for (p, pN) reactions: Kinematically inclusive, semi-inclusive, and fully exclusive cross sections

R. Crespo,[1,2,*] E. Cravo,[3] and A. Deltuva[4]

[1]*Departamento de Física, Instituto Superior Técnico, Universidade de Lisboa, Av. Rovisco Pais 1, 1049-001 Lisboa, Portugal*
[2]*Centro de Ciências e Tecnologias Nucleares, Universidade de Lisboa, Estrada Nacional 10, 2695-066 Bobadela, Portugal*
[3]*Centro de Física Computacional, Departamento de Física, Faculdade de Ciências, Universidade de Lisboa, Edifício C8, Campo Grande, 1749-016 Lisboa, Portugal*
[4]*Institute of Theoretical Physics and Astronomy, Vilnius University, Saulėtekio al. 3, LT-10257 Vilnius, Lithuania*

(Received 20 September 2016; revised manuscript received 31 October 2018; published 23 May 2019)

Background: Nucleon knockout reactions have been previously used to extract single particle information from nuclei. The analysis of nucleon knockout from a stable projectile in the collision with a proton target and the comparison with the experimental data is a key test for the reaction and structure models used to evaluate the reaction observables.
Purpose: We analyze p and n knockout from ^{12}C, assuming that only the heavy fragment or core C (taken as inert), the knockout particle N, and the proton target p participate in the collision process with the aim of (i) getting insight to the dominant kinematic conditions of the emitted particles; (ii) clarifying the dynamics of the reaction; (iii) exploring the isospin dependence (here p and n knockout) of the calculated reaction cross sections.
Method: We solve three-body Faddeev/Alt-Grassberger-Sandhas (Faddeev/AGS) equations for transition operators and calculate kinematically fully exclusive, semi-inclusive, and inclusive cross sections.
Results: We show that (i) the dominant final-state kinematic conditions are consistent with the assumption of quasifree scattering reaction mechanism; (ii) the distortions due to higher order multiple scattering terms depend on the final-state kinematics, and the N-C and p-C final state interaction provide significant effects in the calculated observables; (iii) the twofold energy–polar angle and polar angle–polar angle cross sections exhibit distinct p- and n-knockout behaviors. Finally we also show that the Faddeev/AGS formalism is able to a certain extent to reproduce the available experimental data for the p knockout.
Conclusions: Kinematically fully exclusive measurements of p and n knockout are needed to rigorously assess the role of the distortion, as it cannot be taken into account as an overall reduction factor. This is a prerequisite for a reliable understanding of the structure of the projectile and the reaction mechanism. In addition, realistic interactions inferred from *ab initio* structure models are needed for analyzing experimental data.

DOI: 10.1103/PhysRevC.99.054622

I. INTRODUCTION

One-nucleon knockout reaction in inverse kinematics is a process of removing a nucleon from an incident projectile by its interaction with a target. It has been used as a tool for investigation of the single particle (SP) properties of the projectile nucleus. The extraction of projectile structure information from experiments requires a full understanding of the reaction dynamics. The approach to the latter is often based on assumptions and approximations for which validation is required. One- and two-nucleon knockout reactions have attracted a great deal of attention [1–4].

In this paper, we comprehensively examine the dynamics of nucleon knockout reactions from a projectile with a proton target, within the three-body Faddeev/Alt-Grassberger-Sandhas (Faddeev/AGS) framework [5,6] that has been previously applied to the study of the breakup of loosely bound particles and nucleon knockout from stable and exotic nuclei [7–10]. This reaction approach can be viewed as a multiple scattering expansion in terms of the off-energy-shell transition amplitudes for each interacting pair, thereby including all higher order rescattering terms. The single scattering term between the valence particle/knockout nucleon and the target proton is known as the plane wave impulse approximation (PWIA). The distorted-wave impulse approximation (DWIA) [11] includes an incomplete set of higher order terms that yield significant corrections to the PWIA. Recently, it was shown also in the Faddeev/AGS formalism that significant distortions to the PWIA occur, particularly as a result of higher order rescattering effects between the knockout nucleon and the heavy fragment [9,10,12]. These distortions arise from subtle cancellations between the single scattering contribution that result from the collision between the heavy fragment and the target proton, and higher order multiple scattering terms. The integrated effect of distortions can be quantified by the relative difference between the converged multiple scattering total cross section result (here denoted

*raquel.crespo@tecnico.ulisboa.pt

as FADD) and the PWIA, $D = 1 - \mathcal{R}$ (where $\mathcal{R}$ is the ratio between the FADD and the PWIA total cross sections). It was found [9] that this integrated distortion has a nearly logarithmic dependence on the separation energy of the knockout nucleon for a given angular momentum of the occupied shell. In addition, the calculated ratio of the FADD to the PWIA cross section shows a roughly linear dependence on the neutron-proton asymmetry parameter. Moreover, the calculated PWIA fragment momentum distribution, when renormalized by the ratio $\mathcal{R}$, was found not to fit the details of the FADD result. This indicates that distortion effects may not be taken into account as an overall renormalization for kinematically exclusive or semi-inclusive cross sections.

The analysis of knockout reactions in inverse kinematics at high energies has often been carried out assuming that the quasifree scattering (QFS) with subsequent distortion is the dominant reaction mechanism [13,14]. As the name indicates, the QFS mechanism is governed by the free scattering of two particles. This relies on the drastic assumption that only a limited number of particles participate in the scattering process. For (p, pN), the QFS mechanism assumes that the heavy fragment HF (the projectile with a hole state), the proton target, and the emitted nucleon are the only degrees of freedom that need to be considered in the scattering process. Therefore the light particles (LPs) are expected to emit predominantly in the same plane with the opening angle close to the free NN scattering angle of 90°. Moreover it is also expected that the PWIA, after renormalization by an overall distortion factor (that is produced by higher order multiple scattering contributions), can render a good approximation of the calculated cross sections. The aforesaid conditions have never been tested by an exact theory able to predict three-body kinematically inclusive to fully exclusive cross sections. Assuming that the overwhelming many-body problem can be reduced to a three-body one, we present the calculated kinematically inclusive to fully exclusive reaction cross sections for the knockout of a nucleon (proton/neutron) that result from the collision of a projectile with a proton target.

We aim in this paper to get insight (i) on the dominant kinematic conditions of the emitted particles, and (ii) on the few-body dynamics of the reaction: the detailed role of distortions in kinematically fully exclusive cross sections due to higher order multiple scattering contributions and the role of final-state interaction (FSI) in particular; this has never been addressed from a theoretical point of view. In addition, we also aim (iii) to study the isospin dependence of the knockout cross sections by comparing p and n knockout.

Our working example will be the analysis of nucleon knockout from ^{12}C at high energies of approximately 400 MeV/u for which experimental results have already been obtained via inverse kinematics [14].

The present study is relevant to the knockout experiments using a nuclear probe that are currently performed at radioactive ion beam facilities, as well as to future research developments envisaging one- and two-nucleon knockout experimental studies at high and intermediate projectile energies (as, for example, conducted at FAIR/GSI/Germany and RIKEN/Japan). Our findings also pertain to knockout studies using electron beams.

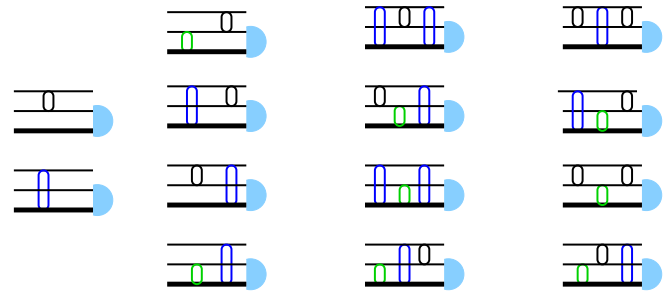

FIG. 1. Diagrammatic representation of the multiple scattering expansion of the Faddeev/AGS formalism viewed in terms of the transition amplitude of each interaction pair to third order. The first term of the expansion represents the PWIA.

II. REACTION FRAMEWORK

The description of the standard Faddeev/AGS equations can be found in many works, e.g., [8]. For the sake of clarity, some of the details of the framework are reproduced here.

Let us consider the knockout of a nucleon N, from a projectile $(A = C + N)$ resulting from its collision with a proton target. We formulate the three-body scattering problem in the Hilbert space $\mathcal{H}_{C+N+p}$ for $C + N + p$ free relative motion where the core C can be either in the ground state or in a low lying excited state. In other words, core dynamical excitations during the collision process or highly excited states above evaporation are not taken into account in this truncated Hilbert space. In addition, in the case of the proton knockout, we only include the Coulomb interaction between the core and the target proton. We also neglect relativistic effects.

In this section we further address the reaction mechanisms for nucleon knockout, in particular, the physical content of the QFS mechanism.

A. Faddeev/AGS formalism

The three-body Faddeev/AGS reaction approach is an exact nonrelativistic formalism where the transition amplitudes leading to the observables are evaluated using two-body transition operators for all three pairs.

These terms are represented in Fig. 1 where the top line represents the target proton, the middle line represents the knockout nucleon, and the thick bottom line represents the heavy fragment or core (assumed here to be in a fixed internal state).

The term where the target proton scatters from the knockout particle is standardly defined as the PWIA. Distortion effects with respect to PWIA are a result of the combined contribution from the p-core single scattering and higher order multiple scattering terms. At high energies subtle cancellations occur between the p-core single scattering and higher order multiple scattering terms [9,10]. Approximate treatments to the multiple scattering expansion may introduce artificial effects into these cancellations. The corrections to the PWIA include contributions that are due to rescattering between the knockout nucleon and the core.

The multiple scattering contributions where the p-core and N-core transition amplitudes appear in the last scattering

(p-core and N-core FSI respectively) are singled out in Fig. 2. We note that the N-core rescattering and p-core FSI contributions are entangled and cannot be treated separately. The Faddeev/AGS reaction framework is a very powerful tool to gain insight into the importance of the above contributions to the calculated cross sections.

The kinematically fully exclusive knockout/breakup cross sections are measured in the laboratory (LAB) system. The spherical coordinate system is chosen to coincide the z axis with the beam direction. We take the two detected particles to be the knockout nucleon (N) and a Z particle [which can be either the target proton ($Z = p$) or the heavy fragment ($Z = C$)] and define $\overline{Z}$ as the undetected particle. The direction of any outgoing particle is given by the polar and azimuthal angles $\Omega_i = (\theta_i, \phi_i)$.

The kinematically fully exclusive cross section can be calculated for any pair of particles, e.g., the light emitted fragments (the target proton and the knockout valence nucleon) or the knockout particle and the heavy fragment [8] as

$$\frac{d^5\sigma}{d\Omega_N d\Omega_Z dS} = (2\pi)^4 \frac{m_N + m_Z}{K_{\rm LAB}} m_{\overline{Z}} m_N m_Z K_Z \left\{ |T^{0\alpha}|^2 \frac{K_N^2}{|(m_N + m_{\overline{Z}})K_N - m_N(\mathbf{K}_{\rm LAB} - \mathbf{K}_Z)\cdot \hat{\mathbf{K}}_N|} \left[1 + \left(\frac{m_Z K_N}{m_N K_Z} \frac{dK_N}{dK_Z} \right)^2 \right]^{-1/2} \right\}, \tag{1}$$

where the transition amplitude $T^{0\alpha}$ can be evaluated from the multiple scattering expansion represented in Fig. 1, and the arc length S is related to the LAB energies E_N and E_Z of the two detected particles as summarized in the Appendix.

The threefold energy-angle cross section for any of the particles in the final state ($\tau = p, N, C$), $\frac{d^3\sigma}{d\Omega_\tau dE_\tau}$ can be calculated as described in [8]. In view of recent developments at the radioactive beam facilities it is now possible to measure twofold cross section observables such as the polar-polar angle cross section $\frac{d^2\sigma}{d\theta_N d\theta_p}$ and the azimuthal-polar angle cross section $\frac{d^2\sigma}{d\phi\, d\theta_N}$ ($\frac{d^2\sigma}{d\phi\, d\theta_p}$) for the knockout nucleon (target proton) with $\phi = \phi_N - \phi_p$.

Measurements of the heavy core momentum distribution have been used to obtain information about single particle properties of the knockout particle. Theoretically, the kinematically semi-inclusive transverse momentum distribution for any measured particle can be readily calculated from the energy-angle cross sections as described in Ref. [8].

The total cross section for the knockout of a nucleon is obtained from further integration. In Ref. [9] we have introduced an integrated cross section to quantify the distortion effects as the relative difference between the calculated PWIA ($\sigma_{\rm PWIA}$) and FADD ($\sigma_{\rm FADD}$) total cross sections, the ratio $\mathcal{R}$, and the distortion parameter $D = 1 - \mathcal{R}$ where

$$\mathcal{R} = \frac{\sigma_{\rm FADD}}{\sigma_{\rm PWIA}}. \tag{2}$$

Some relativistic corrections to these parameters can be expected. The ratio parameter $\mathcal{R}$ represents the integrated effect of higher order multiple scattering (MS) contributions. In the limit where the the multiple scattering corrections do not change the PWIA distribution of the calculated observables, this ratio represents a global renormalization factor to the PWIA result. In general, higher order multiple scattering effects might not be taken completely into account through an overall renormalization factor. The value of the ratio parameter depends on how accurately these higher order contributions are evaluated. In addition, it might depend on the choice of the particle interactions. We shall return to this discussion later in the paper. The Faddeev/AGS formalism allows us to explore to what extent higher order MS contributions to the PWIA can be replaced by an overall renormalization factor.

The single particle (sp) total cross section, evaluated considering a core with spin I_C^π coupled with a nucleon with quantum numbers $n\ell j$ and unit spectroscopic factor, is evaluated here within the adopted standard Faddeev/AGS reaction approach and denoted as $\sigma_{\rm sp}(I_C^\pi, n\ell j)$. The theoretical cross section for this configuration, $\sigma_{\rm theo}(I_C^\pi, n\ell j)$ is obtained multiplying the SP cross section with a spectroscopic factor. This is obtained from the ratio between the experimental to theoretical SP total cross section for the case of proton knockout from the ^{12}C projectile.

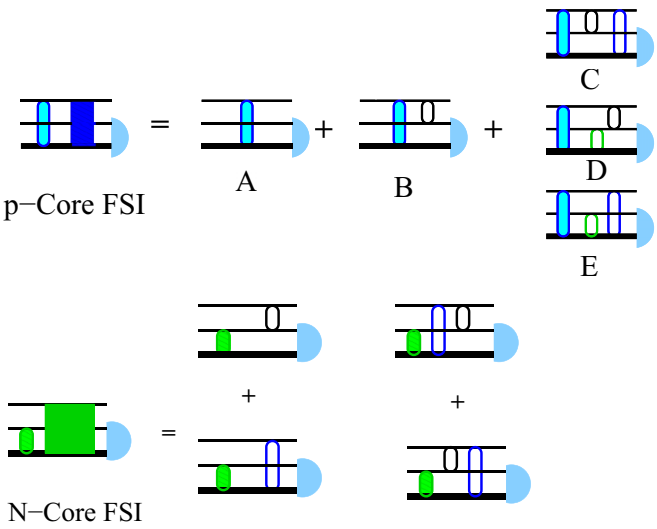

FIG. 2. Diagrammatic representation of the multiple scattering contributing terms (up to third order) to the p-core FSI and N-core FSI.

B. Reaction mechanisms

For clarification we discuss here the reaction mechanisms that can arise when removing a nucleon from a projectile in

a collision with a target (here a proton). We also review the different notation used for these reaction mechanisms. The Faddeev/AGS formalism *takes simultaneously into account all these mechanisms and its possible couplings*.

1. Electromagnetic dissociation or Coulomb breakup

This process is due to the Coulomb interaction between the heavy fragment and the target. Both nuclear and Coulomb interactions with their interference can be included into the Faddeev/AGS formalism. This process becomes dominant in the case of heavy target and therefore is comparatively negligible in the present case of the proton target.

2. Resonance and nonresonance nuclear breakup

This is an important reaction mechanism at intermediate energies and is often called nuclear inelastic scattering into resonant or nonresonant continuum or as elastic breakup. To include this into the Faddeev/AGS reaction formalism, the interactions between the ejected nucleon and heavy fragment have to reproduce the desired resonant features [15]. In some cases resonant transitions to the continuum were found to be important or even dominant in the case of Halo nuclei [15,16]. The ground state of ^{12}C lies 7.3 MeV below the α threshold. The Hoyle state just above this threshold has a strong correlated α structure and some evidence suggests that these correlations are also present in the ground state as discussed in Ref. [17] and references therein. We do not attempt to include here the coupling to these states.

3. pN quasifree scattering mechanism

This reaction mechanism is often named in the literature as inelastic breakup or as absorption or stripping. The detailed analysis of this reaction mechanism is the main goal of the present paper.

For nucleon knockout from a nucleus A the assumption that the QFS mechanism is dominant relies on the premises that (i) only a limited number of particles participate in the scattering process, that is, the heavy fragment (the projectile with a hole state), the proton target, and the emitted nucleon, and (ii) the scattering cross section is determined by the free proton-nucleon cross section that must be subsequently renormalized due to the distortion.

We discuss how the present work can provide theoretical insight on the assumption that the scattering is determined by the free proton-nucleon cross section.

We assume in this section direct kinematics $A(p, pN)$, although current experiments at RIB facilities are performed in inverse kinematics. The results discussed here are however independent of the kinematics that is used.

The QFS mechanism is expected to be dominant for small momentum transferred to the heavy fragment. Therefore the momentum of the heavy fragment, i.e., of the projectile core, in the center of mass of the projectile is equal to the momentum of the struck nucleon within the projectile (with minus sign). The pN QFS reaction mechanism without distortion is represented diagrammatically in Fig. 3.

Quantitatively, the undistorted QFS cross section for nucleon knockout can be factorized as the product of two terms,

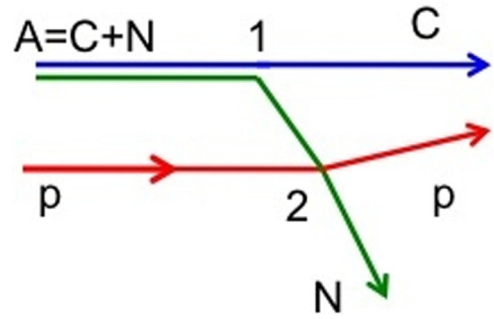

FIG. 3. QFS diagram for the N-knockout reaction $A(p, pN)$.

related to the two vertices of Fig. 3, namely (i) the momentum-space wave function $\mathcal{P}(\mathbf{K}_C)$ for the relative N-C motion (vertex 1), and (ii) the cross section $\frac{d\sigma}{d\Omega_{pN}}(\mathbf{K}_p, \mathbf{K}_N)$ for the reaction $p + N \to p + N$ (vertex 2). Thus, the QFS transition amplitude in Eq. (1) has to be replaced by

$$\left|T^{0\alpha}_{\rm QFS}\right|^2 = \mathcal{R}|\mathcal{P}(\mathbf{K}_C)|^2 \frac{1}{4\pi^4 m_N^2} \frac{d\sigma}{d\Omega_{pN}}(\mathbf{K}_p, \mathbf{K}_N). \qquad (3)$$

Here the factor $\mathcal{R}$ from Eq. (2) approximately accounts for the distortion. In other words, it is assumed that multiple scattering corrections do not change the shape of the differential cross section, only renormalize it. Deviations from that shape indicate the limitations of the QFS assumption. Note that $|\mathcal{P}(\mathbf{K}_C)|^2$ gives the momentum distribution of the core in the projectile [11].

Clearly from Eq. (3) the dynamics of the reaction is governed by vertex 2 and therefore the light particles are expected to be emitted with coplanar kinematics, and with an opening angle that is close to the free pN scattering angle but reduced due to the internal motion of the knockout particle. The factorization approximation in Eq. (3) underpins the possibility of extracting a spectroscopic factor.

In the exact three-body Faddeev/AGS formalism the scattering cross sections are calculated from Eq. (1) and cannot be expressed in the simplified factorized form given by Eq. (3). This factorization can only be achieved in the PWIA limit and taking the NN transition amplitude at fixed energy and on shell. In this paper we aim to investigate to what extent the Faddeev/AGS result retains the dominant kinematic conditions that follow from Eq. (3) and to what extent the calculated (in particular kinematic fully exclusive) cross sections using the Faddeev/AGS equations can be approximated by the PWIA result multiplied by a distortion factor due to higher order multiple scattering terms, as defined in Eq. (2).

III. STRUCTURE MODEL

In order to study the reaction mechanism for nucleon knockout from ^{12}C we expand the projectile wave function in terms of the heavy fragment ground state and some low lying excited states as

$$\begin{aligned} |^A X\rangle = {} & \mathcal{Z}^{1/2}(3/2^-_1)\,|^{A-1}X(3/2^-_1)\otimes 1p_{3/2}\rangle \\ & + \mathcal{Z}^{1/2}(3/2^-_2)\,|^{A-1}X(3/2^-_2)\otimes 1p_{3/2}\rangle \\ & + \mathcal{Z}^{1/2}(1/2^-_1)\,|^{A-1}X(1/2^-_1)\otimes 1p_{1/2}\rangle, \end{aligned} \qquad (4)$$

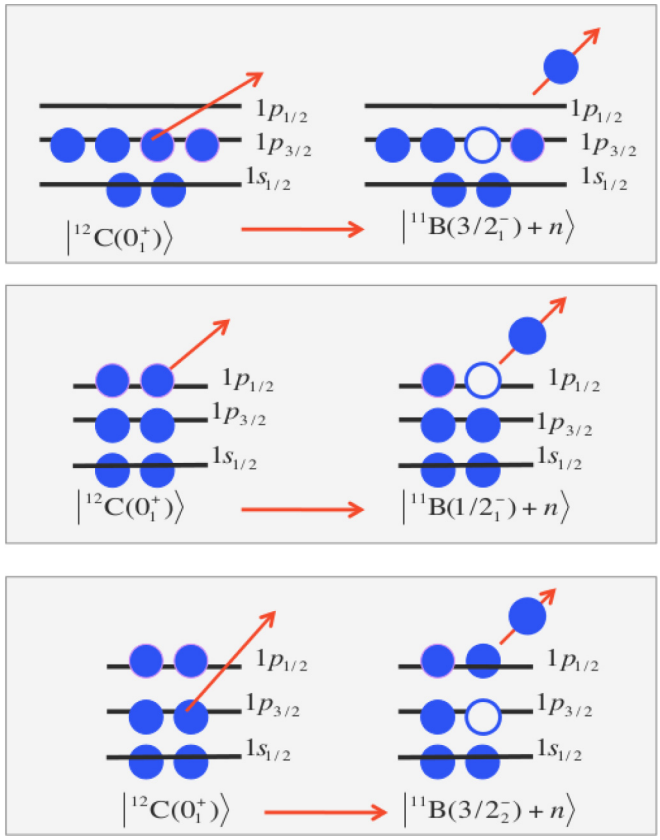

FIG. 4. Shell model scheme for the $p-$ knockout from ^{12}C leading to the ground state $(3/2_1^-)$ and the two excited states $(1/2_1^-)$ and $(3/2_2^-)$ of ^{11}B.

where X represents the carbon or boron isotope and $\mathcal{Z}$ are spectroscopic factors that can be obtained from the comparison with the experimental data.

In this paper we mainly consider the contribution of the nucleon knockout from the valence $1p_{3/2}$ shell. For the purpose of comparison with the $(p, 2p)$ experimental data we shall also consider the ^{11}B heavy fragment in the low lying excited states $^{11}\mathrm{B}(3/2_2^-)$ and $^{11}\mathrm{B}(1/2_1^-)$ represented schematically in Fig. 4 within a simplified picture where the knockout particles are removed from occupied shells.

It is assumed that this observable is given by the incoherent sum of all contributions.

IV. INTERACTIONS

Our working example is the analysis of nucleon knockout from ^{12}C at 400 MeV/u.

Before solving the Faddeev/AGS equations we need to specify the three pair interactions, that is, the N-p (knockout nucleon proton), N-C (knockout nucleon core), and p-C (target proton core). We take the realistic nucleon-nucleon CD Bonn potential [18] for the proton-nucleon particle pair. Note that the p-p interaction acts in isospin triplet partial waves only while the p-n interaction acts also in isospin singlet partial waves, e.g., $^3S_1 - {}^3D_1$, $^1P_1$, $^3D_2$, etc., that yield important contributions. The results presented in this paper do not change significantly with respect to the choice of a different realistic p-N interaction.

TABLE I. Nucleon-core optical potential models used in the present work with the parameters evaluated at the given energy.

Model	Ref., remarks	Energy (MeV)
BAU	[19], set II	400
BAUI	[19], set I	400
J	[20]	200
KD	[21]	200

Obviously, in the partial wave corresponding to the initial valence-core bound state the valence-core potential must be real in order to support the desired bound state. We take a central Woods-Saxon interaction with standard radius $R = 1.25A^{1/3}$ fm and diffuseness $a = 0.65$ fm, and adjust the depth to reproduce the binding energy [10]. This binding energy is calculated from the sum of the excitation energy of the heavy fragment $(A-1)$ with the nucleon separation energy of the projectile A, that is

$$|-\epsilon_N| = E_x(A-1) + S_N(A). \tag{5}$$

The ^{12}C nucleon separation energies are $S_n = 18.722$ MeV and $S_p = 15.957$ MeV.

We shall consider the p- and n-knockout leading to the heavy fragment ground state. In addition we also consider the p knockout leading to two excited states $^{11}\mathrm{B}(1/2^-; E_x = 2.125$ MeV) and $^{11}\mathrm{B}(3/2_2^-; E_x = 5.020$ MeV).

The potentials between nucleons and core in all other waves are far less constrained, and may have both real and imaginary components. We are not aware of nucleon-^{11}B and nucleon-^{11}C data at the considered energy that would help to fix the potentials. However, one may expect proton-^{12}C data and resulting potentials to provide some guidance. To investigate the uncertainties of the calculated cross sections associated with the choice of the optical potential describing the N-core interaction in other partial waves, and the target proton-core interaction, we consider several phenomenological sets. We consider the Bauhoff (BAU) optical potential parametrizations (sets I and II) [19], obtained by

TABLE II. PWIA and Faddeev/AGS SP total cross sections for p and n knockout from the ^{12}C ground state calculated using BAU-J and KD-KD parametrizations. Also shown are the results without the p-core and N-core FSI. All cross sections are given in units of mb. The renormalization factors $\mathcal{R}$ defined in Eq. (2) are given in the last line.

	$(p, 2p)$		(p, pn)	
	BAU-J	KD-KD	BAU-J	KD-KD
PWIA	21.8	21.8	29.3	29.3
FADD	6.02	8.54	7.75	11.6
p-CnoFSI	42.6	27.7	46.7	30.6
N-CnoFSI	42.6	27.7	48.6	33.1
$\mathcal{R}$	0.276	0.392	0.265	0.396

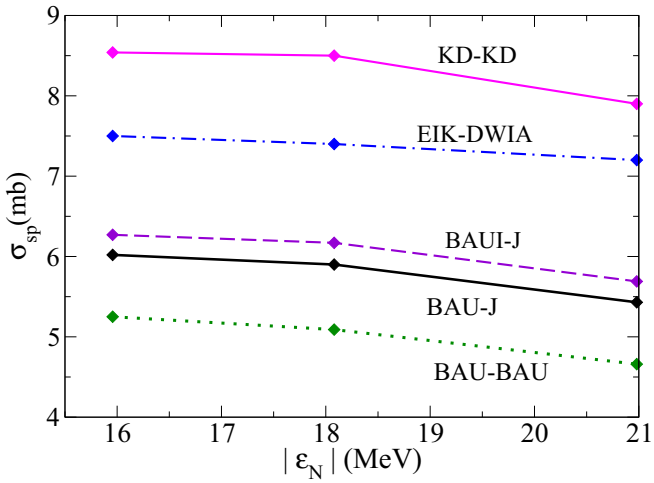

FIG. 5. Faddeev/AGS single particle total cross sections for p knockout using different potential parametrizations for the ground state ($3/2^-_1$) and the two excited states ($1/2^-_1$) and ($3/2^-_2$) represented here as a function of the nucleon separation energy. Also shown the EIK-DWIA results for the same final states.

fitting proton-^{12}C elastic scattering at 400 MeV, and the Jones (J) parametrization [20], obtained by fitting proton-^{12}C elastic and inelastic scattering at intermediate energies. Finally, we consider also the Koning-Delaroche (KD) potential, where the parameters are taken from the global optical potential parametrization [21] for n and p scattering from

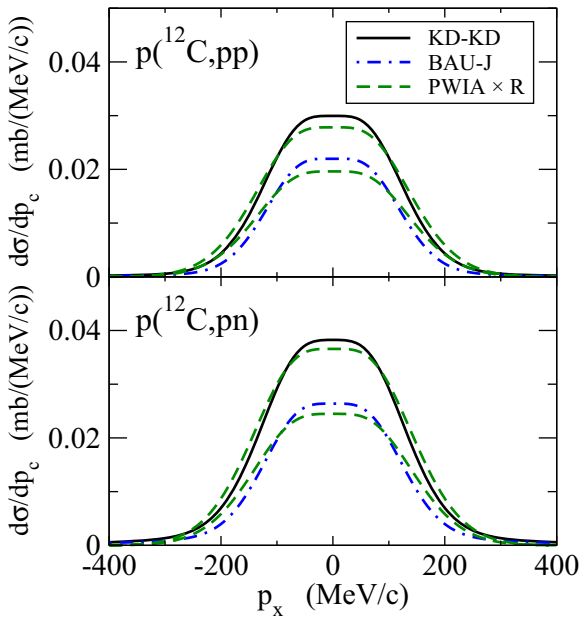

FIG. 6. Heavy fragment ground state transverse momentum p_c distributions along the Cartesian X axis for p (top) and n knockout (bottom). The solid and dot-dashed lines represent the FADD and the dashed lines represent the renormalized PWIA cross sections. The ratios $\mathcal{R}$ of the FADD to the PWIA total cross section are given in Table II.

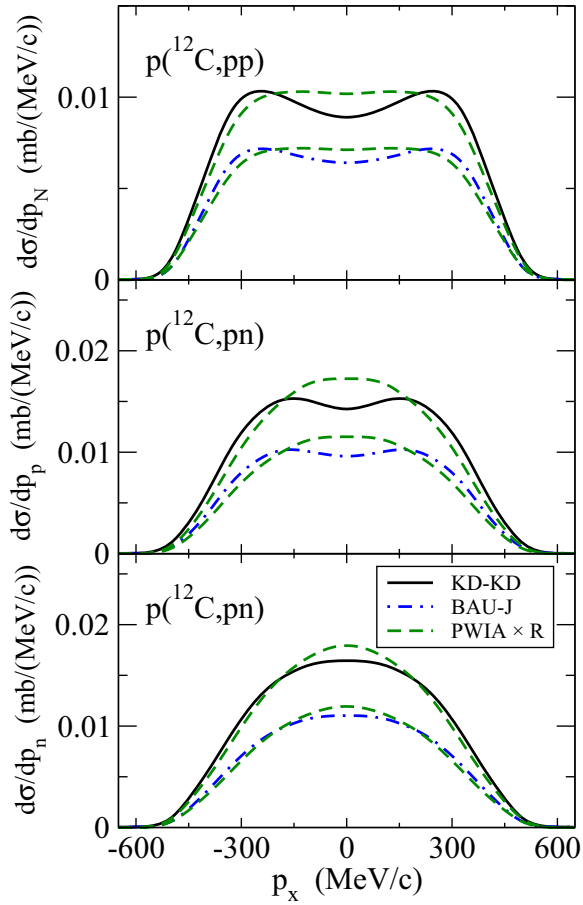

FIG. 7. Nucleon transverse momentum along the Cartesian X axis p_x distributions for p and n knockout. The middle and bottom graphs show the momentum distributions for the target proton and the neutron, respectively. The solid and dot-dashed lines represent the FADD and the dashed line represents the renormalized PWIA cross sections. The ratios $\mathcal{R}$ are given in Table II.

(near-)spherical nuclides in the mass range $24 <= A <= 209$ in the energy range from 1 keV to 200 MeV. Thus, this parametrization is not really designed for nuclei $A < 24$, and does not fit in detail the proton elastic scattering from ^{12}C at 400 MeV, but has been used for systematic studies along the nuclear landscape [9,22]. The comparison should provide a maximization of the error associated with the uncertainties of the optical potential parametrizations.

All the parameters of the above potentials are given in the corresponding Refs. [19–21]; we only have to use $A = 11$. Furthermore, the Faddeev/AGS framework generally requires energy independent potentials. Thus, we have to fix the energy for each parametrization. Commonly used choices are either reaction energy, or half of it, that is, 400 or 200 MeV in the present case. Again, we make several choices to study the associated uncertainties, and the used models are listed in Table I. The predictions will be labeled by two models, the first one corresponding to the p core and the second one corresponding to the N core pair, e.g., BAU-J means Bauhoff (Jones) parametrization for p core (N core).

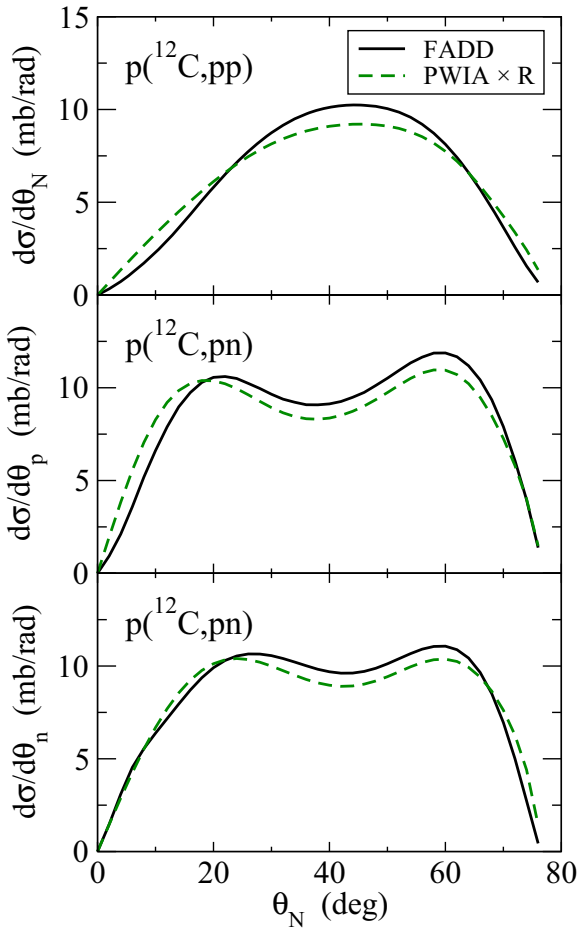

FIG. 8. Angular cross sections for p and n knockout. The middle and the bottom graphs show the cross sections for the target proton and the neutron, respectively. The solid and dashed lines represent the FADD and the renormalized PWIA cross sections, respectively, with $\mathcal{R}$ given in Table II. The KD-KD optical potential parametrization was used.

V. RESULTS

We solve the Faddeev/AGS equations and calculate the cross sections for a projectile incident beam of 400 MeV/u.

The numerical solution is performed in the momentum space, after partial wave decomposition and discretization of all momentum variables. The calculations include N-p partial waves with orbital angular momentum $L \leqslant 8$, n-C partial waves with $L \leqslant 8$, and p-C partial waves with $L \leqslant 16$. The total three-particle angular momentum is $J \leqslant 50$; there are no additional limitations on the spectator orbital momenta. We include the nuclear interaction between all three pairs. The Coulomb interaction between the target proton and the heavy fragment is included as described in Ref. [23]. Although the results for the proton knockout suffer from the uncertainty that is inherent to the incompleteness of the Coulomb interaction, this should not affect the estimates and qualitative conclusions that we present.

In the following sections we show some calculated cross sections that can be measured in current experimental facilities. In addition, we discuss kinematically fully exclusive cross sections that will be measured in the future.

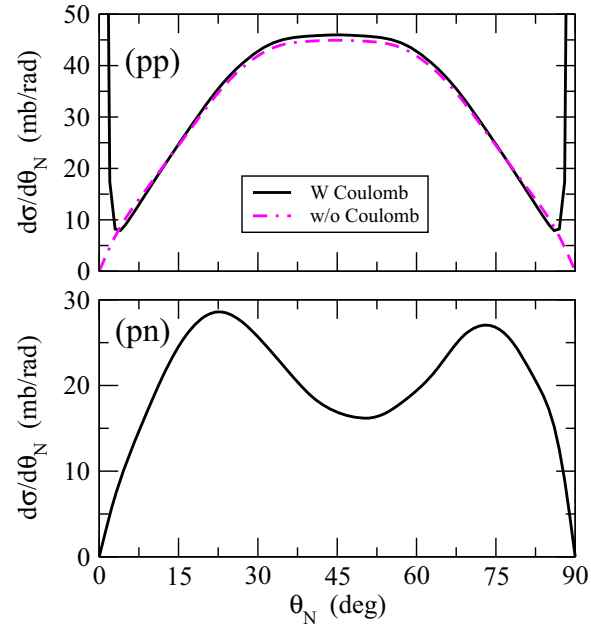

FIG. 9. pp (top) and pn (bottom) elastic cross sections at 400 MeV beam energy. The dashed line for pp represents the angular distribution without the Coulomb interaction.

A. Kinematically inclusive cross sections

In this section we discuss the kinematically integrated cross sections. The PWIA theoretical total cross section for n knockout to the $^{11}C(3/2^-)$ g.s. is $\sigma_{PWIA} = 29.3$ mb. For p knockout the calculated single particle total cross section to the $^{11}B(3/2^-)$ g.s. is $\sigma_{PWIA} = 21.8$ mb.

In Table II we compare the total single particle cross sections for p and n knockout leading to the ground state of the heavy fragment using the BAU-J and the KD-KD interactions with the cross sections evaluated without the p-core and N-core FSI represented in Fig. 2. It follows that the FSI effects provide an important contribution to the total cross section.

In order to have insight on the maximum uncertainty associated with the choice of the parametrizations of the optical potential, the SP total cross sections for p knockout leading to the ground and excited states of the heavy fragment [taking the nucleon separation energy of the projectile A from Eq. (5)] are presented in Fig. 5. The results demonstrate clearly the need of having a reliable description of the optical potential parametrizations. Also shown are the theoretical results taken from [14] using the Eikonal distorted wave impulse approximation (EIK-DWIA) as described in Ref. [14] and references therein. The differences between the two reaction approaches might originate from the interactions.

B. Kinematically semi-inclusive cross sections

In this section we discuss the kinematically semi-inclusive cross sections. In Fig. 6 we show transverse momentum distributions for the heavy fragment. The z axis is taken in the

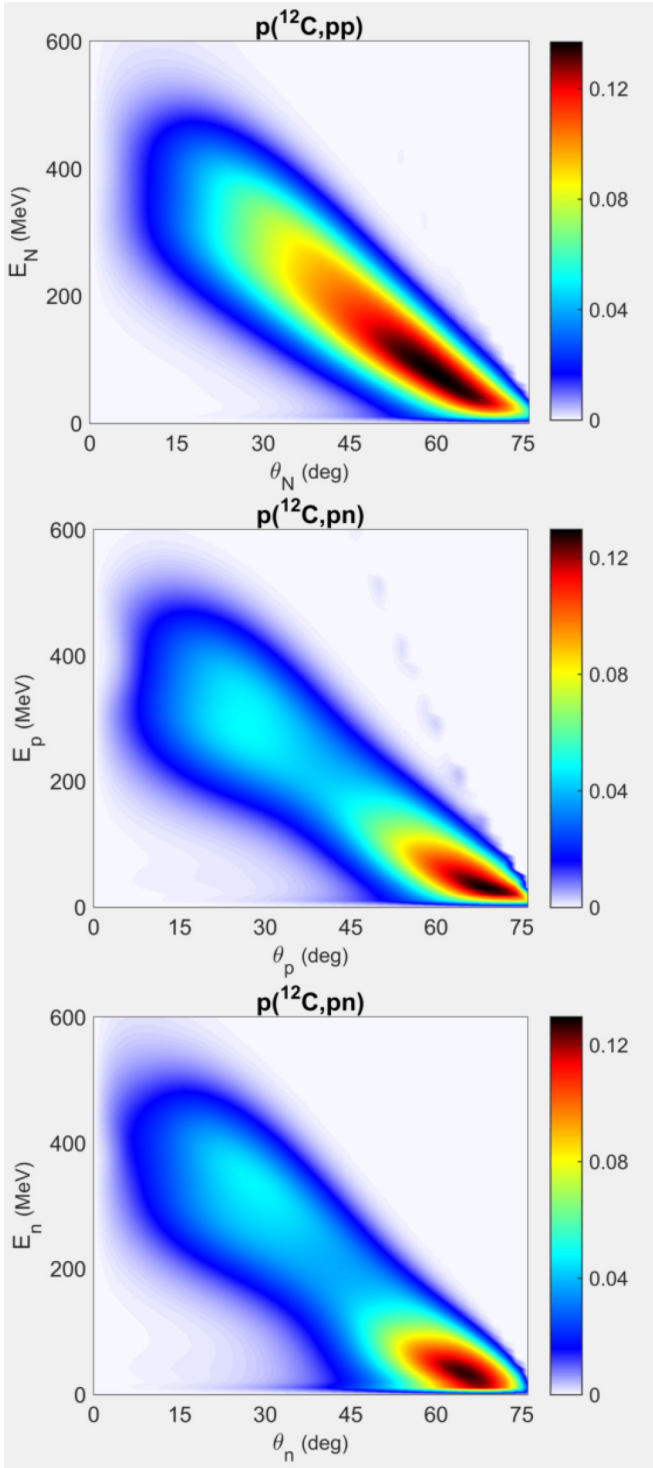

FIG. 10. Contour plot of the energy-polar angle correlation cross section $\frac{d^2\sigma}{dE_p d\theta_p}$ for p knockout and $\frac{d^2\sigma}{dE_N d\theta_N}$ for n knockout. The cross sections are in units of mb/(MeV rad). The KD-KD optical potential parametrization was used.

beam direction. The solid and dot-dashed lines represent the FADD results. The dashed line was obtained from the PWIA renormalized by the ratio $\mathcal{R}$ between the FADD and the PWIA cross section defined in Eq. (2).

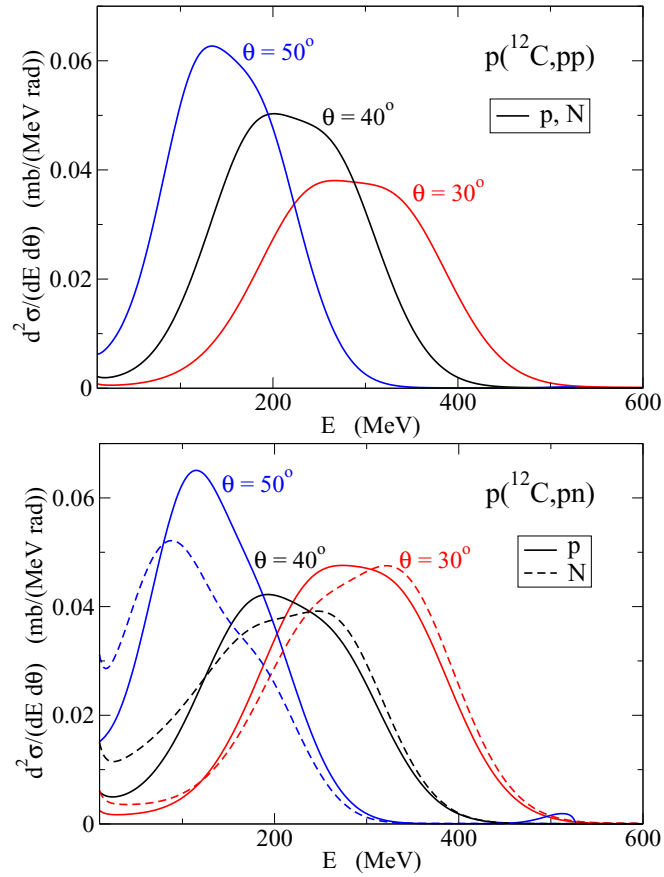

FIG. 11. Calculated $\frac{d^2\sigma}{dE_p d\theta_p}$ (solid line) and $\frac{d^2\sigma}{dE_N d\theta_N}$ (dashed line) at fixed angles θ of the measured particle, for p and n knockout. The KD-KD optical potential parametrization was used.

In Fig. 7 we show the transverse momentum distributions for the light particles (the target proton and the knockout nucleon). It follows from the figures that the renormalized PWIA does not reproduce the FADD result in detail. This indicates that distortion effects may not be accurately taken into account as an overall renormalization of the kinematically semi-inclusive and fully exclusive results. We shall refer to this point later.

In inverse kinematics, if the heavy fragment is bound, it is possible to measure directly the HF momentum distribution in the LAB frame, from reconstruction of its velocity and angles with respect to the incident beam angle, normalized by the measured integrated cross section. For the initial state, and in the projectile rest frame, the internal momenta of the knockout particle and heavy fragment are related as $\mathbf{K}_N = -\mathbf{K}_C$. Under the dominance of the Np QFS reaction mechanism, there is no momentum transfer to the heavy fragment, and therefore the momentum of the heavy fragment in the final state is equal to the internal momentum of the knockout particle. In the limit where distortion can be taken into account as an overall renormalization, and the phase-space factor and the transition amplitude for the light particles can be taken as constant within the range of the energy of the core, then the measured momentum distribution of the heavy fragment can provide information on the internal properties of the knockout particle

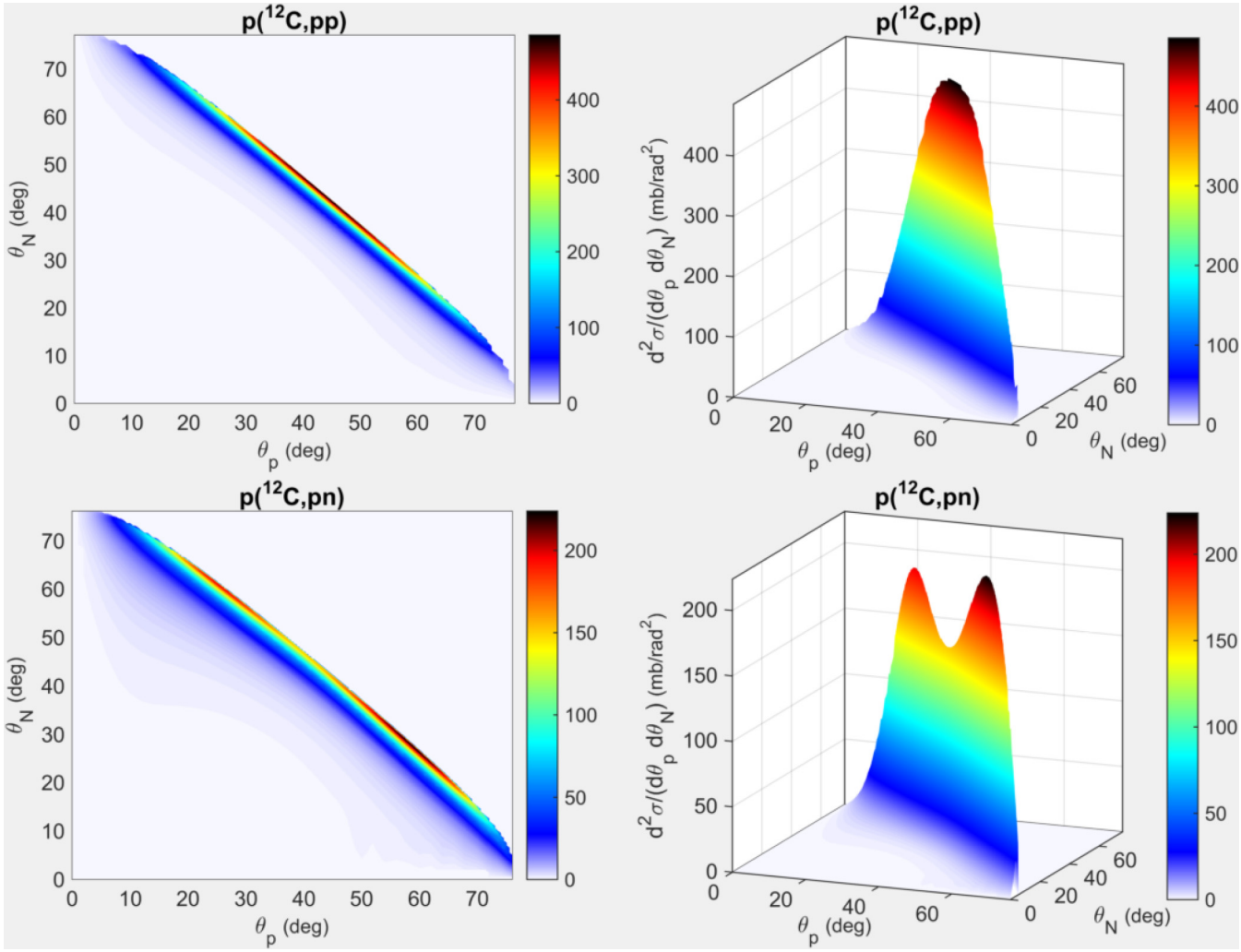

FIG. 12. Contour plot and 3D graphical representations of the angular correlation cross sections $\frac{d^2\sigma}{d\theta_p d\theta_N}$ for p (top) and n knockout (bottom). The cross sections are in units of mb/rad^2. The KD-KD optical potential parametrization was used.

such as its internal and angular momentum. Therefore if the QFS mechanism is dominant the HF momentum distribution represented in Fig. 6 reflects the internal momentum of the knockout particle.

In the limit where the reaction happens at/near the Np QFS kinematic condition one expects a large transfer momentum to the light particles and as result, a broader momentum distribution than the HF distribution as can be seen from Figs. 6 and 7. Therefore, the broader momentum distribution of the light particles is an indicator of the dominance of the QFS reaction mechanism. Nevertheless, the renormalized PWIA does not agree with the FADD result in detail.

In Fig. 8 we show the angular distributions for the semi-inclusive cross section for the knockout nucleon $\frac{d\sigma}{d\theta_N}$ and for the target proton $\frac{d\sigma}{d\theta_p}$ for p and n knockout. The solid line represents the FADD result and the dashed line the renormalized PWIA result. The angular distributions for p knockout has a maximum at LAB polar angles around 45°. For the case of n-knockout the cross sections has a characteristic minimum at around 40° and two maxima at around 25° and 60°.

One notes that the range of the polar angle distribution of the light particles is smaller than the corresponding free case represented in Fig. 9. We identify this effect as a medium effect due to the binding of the knockout nucleon. We note that the free pn angular distribution shows a two-peak structure as a function of the neutron (proton) polar angle with a maximum at θ_n (θ_p) around 20° (70°). For the case of n knockout, the folding of the transition amplitude with the relative wave function and the kinematic factor modifies the polar angle distribution and the maximum value of the cross section is seen at a larger value. Also shown at the top part of Fig. 9 is the angular distribution for the free pp scattering without Coulomb. The curve illustrates that Coulomb interaction effects in pp scattering are only significant at very small or very large proton polar angles.

C. Kinematically twofold cross sections

In Fig. 10 we show the contour plot of the FADD energy-polar angle correlation cross sections for p and n knockout,

$\frac{d^2\sigma}{dE_p d\theta_p}$ (for measured target proton) and $\frac{d^2\sigma}{dE_N d\theta_N}$ (for measured knockout particle). For the case of p knockout, the protons (that are indistinguishable) have a smaller energy at large polar angles, where the cross section is higher. Their energy increases uniformly for smaller polar angles, where the cross section is smaller. Similarly, for the case of n knockout, the target proton and knockout neutron have a smaller energy at large polar angles, where the cross section is higher. However, the energy-angle correlated cross section shows a distinct behavior from the case of p knockout. The cross section does not decrease uniformly with the polar angle of the detected light particle and exhibits a local minimum at around 40°. This behavior is clearly evident in Fig. 11 where we show the energy-angle distribution for given angles of the detected particle (30°, 40°, and 50°).

In Fig. 12 we show the contour plots and 3D graphical representations of the FADD angular cross sections $\frac{d^2\sigma}{d\theta_p d\theta_N}$ for p and n knockout. These polar angle-correlation cross sections result from integrating over the azimuthal angles of each particle. The figure shows that the final state light particles are angle correlated and their opening angle $\alpha = \theta_p - \theta_N$ is close to the QFS value of 90°, and further exhibits a sharp distribution around this value. The broadening of the distribution is connected to the binding of the knockout particle to the heavy fragment. The figure shows that the polar angular correlation cross sections exhibit a distinct isotopic spin behavior. For p knockout the intensity of the angular correlation cross section is a slowly varying function of the angle and attains its zenith when the polar angle pair of the target proton and knockout proton is $(\theta_p, \theta_N) = (42.6°, 44.4°)$. For n knockout the intensity of the polar angular correlation cross section $\frac{d^2\sigma}{d\theta_p d\theta_N}$ has an anisotropic behavior, with a first maximum for $(\theta_p, \theta_N) = (55.1°, 31.1°)$. Obviously, this is due to the differences in pp and pn interactions, the former being limited to isospin triplet states while the latter acts in both isospin singlet and triplet states.

We now analyze in detail the polar angle distribution between the two final state light particles. In Fig. 13 we show the calculated FADD (solid curve) and renormalized PWIA (dashed curve) $d^3\sigma/(d\theta_p d\theta_N d\phi)$ in the coplanar kinematics with $\phi = 180°$ for fixed angles of the target proton, $\theta_p = 42.6°$ and $\theta_p = 55.1°$. In all cases the calculated cross sections show an opening angle correlation close to the QFS value of 90°. This opening angle distribution is essentially independent of the higher order distortion effects. The calculated FADD result is slightly narrower than the renormalized PWIA.

Figure 14 shows the contour plot of the PWIA azimuthal-polar angle correlations for measured nucleon knockout $\frac{d^2\sigma}{d\phi\, d\theta_N}$ and target proton $\frac{d^2\sigma}{d\phi\, d\theta_p}$ with $\phi = \phi_N - \phi_p$ for p and n knockout. The results show that the knockout nucleon and the target proton are correlated in the QFS coplanar kinematics with a maximum distribution around $\phi = \phi_N - \phi_p = 180°$. From the figure follows that the azimuthal angular correlation cross section also exhibits a distinct isotopic spin behavior. While for p knockout the distribution peaks when two final state light particles are located at around 45°, for n knockout the distribution reaches its peak when the knockout neutron is located at around 30° and the target proton is emitted at around 60°.

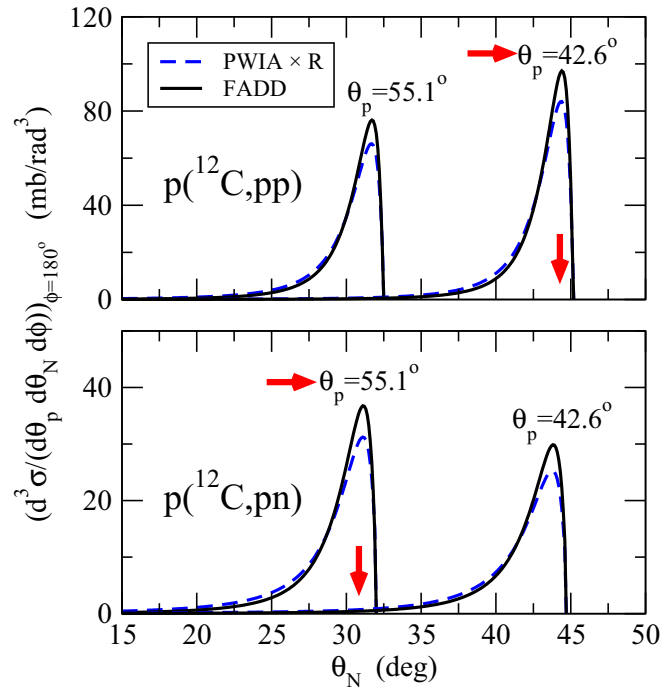

FIG. 13. Angular correlation cross sections $d^3\sigma/(d\theta_p d\theta_N d\phi)$ with $\phi = 180°$ and fixed target proton angles for p (top) and n knockout (bottom). The solid and dashed lines represent the FADD and renormalized PWIA result, respectively, with $\mathcal{R}$ given in Table II. The KD-KD optical potential parametrization was used.

D. Kinematically fully exclusive cross sections

In this section we discuss the kinematically fully exclusive cross section $\frac{d^5\sigma}{dS d\Omega_p d\Omega_N}$, as defined in Sec. II, as a function of the S parameter for coplanar geometry, that is $\phi = \phi_N - \phi_p = 180°$, and for two different polar angle kinematic configurations of the light fragment's final state: configuration 1 with $(\theta_p, \theta_N) = (55.1°, 31.1°)$, and configuration 2 with $(\theta_p, \theta_N) = (42.6°, 44.4°)$. These configurations correspond to polar angle points where the the angular correlation of the two light particles has a maximum for n knockout and p knockout respectively. In addition, we consider two parametrizations of the optical potentials.

The S parameter is represented in Fig. 15 for p and n knockout as a function of particle LAB energies. Clearly, the S parameter is a characteristic of the kinematic configuration and depends also on the binding energy of the knockout particle. The $S = 0$ point is chosen such that it corresponds to the value where the energy of the knockout nucleon has minimum.

Figures 16 and 17 show the kinematically fully exclusive cross section for the two kinematic configurations and parametrizations of the optical potential. To obtain insight into the role of FSI we also show the calculated cross sections without p-core and N-core FSI (see Fig. 2). The ratio of the FADD and PWIA results shown in the figures

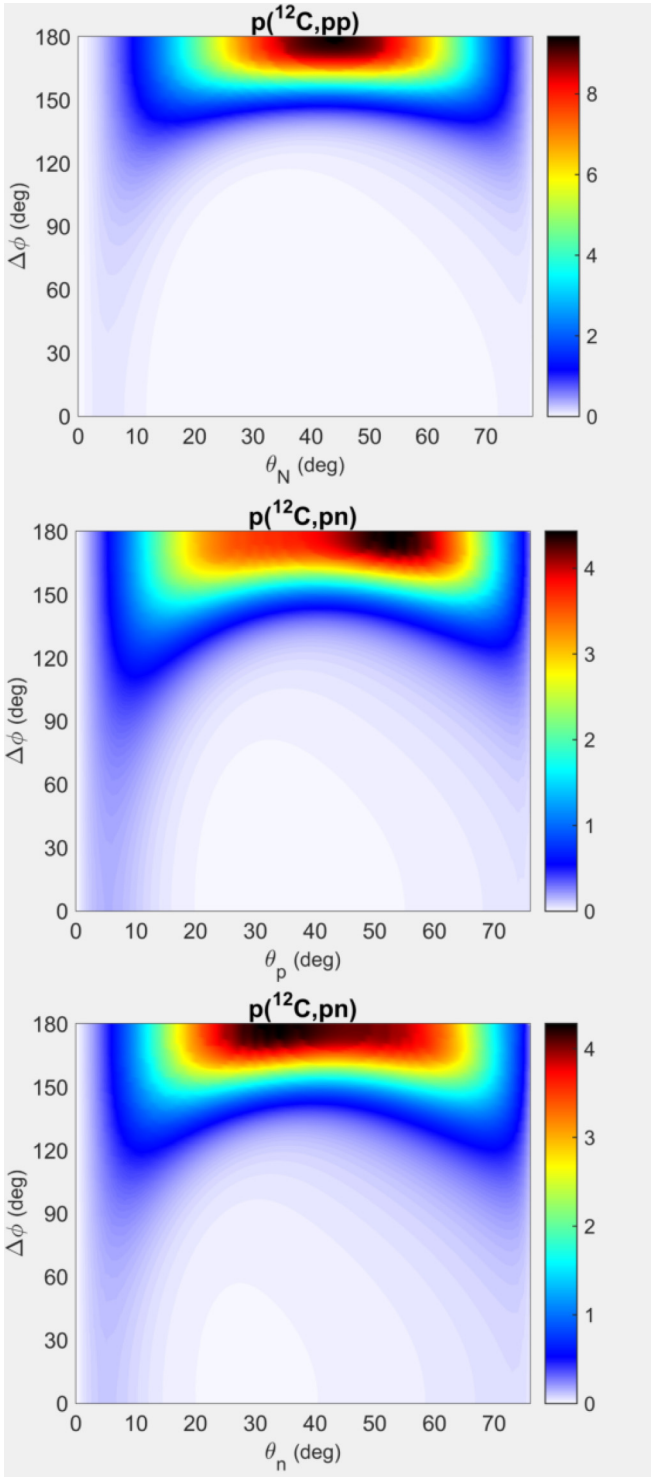

FIG. 14. Contour plot of the PWIA azimuthal angle correlations $\frac{d^2\sigma}{d\Phi d\theta_p}$ and $\frac{d^2\sigma}{d\Phi d\theta_N}$, with $\Delta\Phi = \Phi_N - \Phi_p$ for p and n knockout, where $\Phi_N(\Phi_p)$ is the azimuthal angle for the knockout nucleon (proton). The cross sections are in units of mb/sr. The KD-KD optical potential parametrization was used.

is not a constant for any of the kinematic configurations. Therefore the Faddeev/AGS kinematically exclusive cross section is not related to the PWIA result through a common

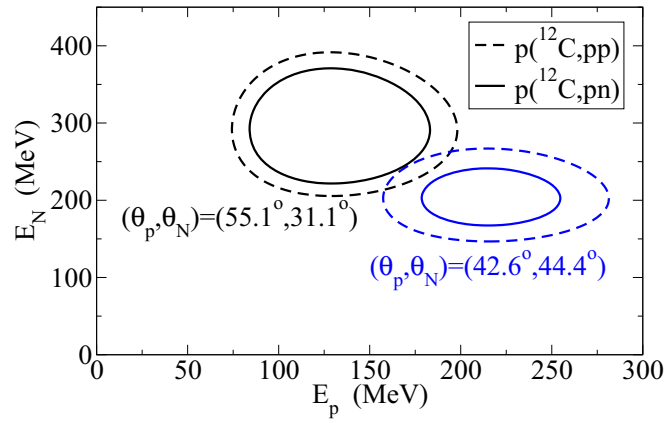

FIG. 15. S parameter for different kinematic configurations as discussed in the text.

integrated renormalization factor. Nevertheless, for p knockout the renormalization remains close to the calculated integrated ratio while stronger deviations occur for neutron knockout with respect to the integrated value. In addition, the ratios between the calculated Faddeev/AGS to the no p-core and no N-core FSI results are essentially constant for p-knockout, but they vary significantly for n knockout. However, in some configurations and in some restricted kinematic region, the deviation from a constant renormalization factor can be minimized. In any case we note that this renormalization factor depends on the configuration, and often deviates significantly from the integrated ratio.

The relative energies between each interacting pair are given at the bottom of Figs. 16 and 17. The proton-core and neutron-core relative energies remain essentially constant as a function of the S parameter for each configuration. Assuming a moderate dependence of the parametrizations of the optical potential we have taken the potentials at a fixed energy of 200 and 400 MeV for the N-C and p-C parametrizations.

The neutron proton relative energy exhibits a more significant variation around the free NN scattering value of $\omega = E/2 = 200$ MeV, and therefore it is important to include in the calculations the energy dependence of the transition amplitude for the light interacting pair. Nevertheless, the neutron proton relative energy remains above 150 MeV in this energy regime and for these kinematic configurations one expects the n-p QFS regime to be achieved without small relative pN energies. Notwithstanding, with the small dependence on the proton-core and neutron-core relative energy, one obtains large p-C and n-C FSI effects that can only be approximated by a renormalization factor in some kinematic configurations and in some restricted phase space.

E. Data analysis of $p(^{12}C, 2p)^{11}B$ at 400 MeV/u

The calculated cylindrical transverse momentum p_{tr} distribution for different optical potential parametrizations is compared with the experimental results of [14] in Fig. 18. The calculated curves result from summing the contributions leading to the ^{11}B core in the ground state $(3/2^-_1)$ and the

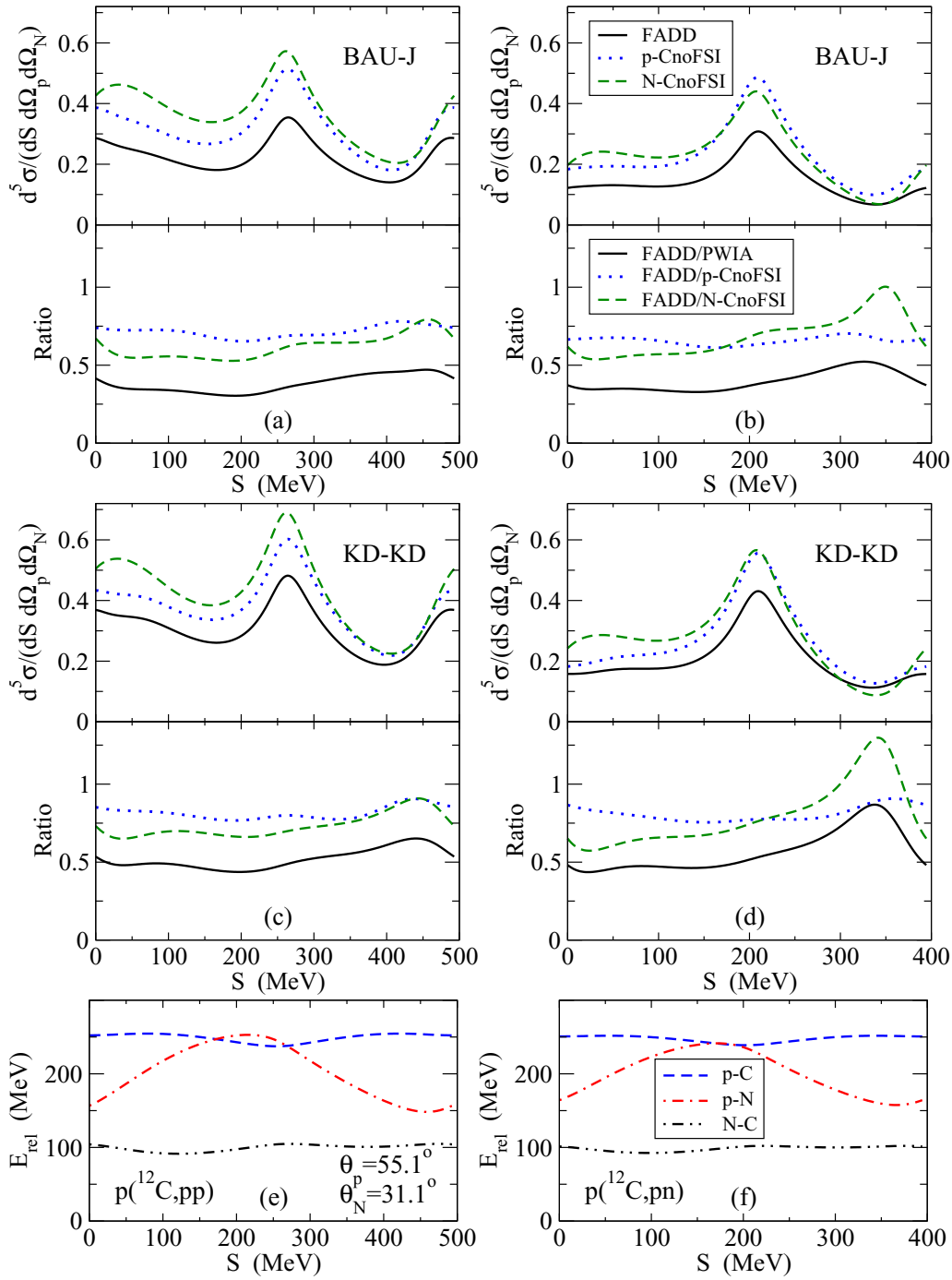

FIG. 16. The top and middle parts of the figure represent the kinematically fully exclusive cross sections as a function of the S parameter, $\frac{d^5\sigma}{dSd\Omega_p d\Omega_N}$, as defined in the text, for fixed polar angles and coplanar geometry, using two different optical potential parametrizations for p (left) and n (right) knockout. Also shown is the ratio between the FADD result and the PWIA approximation. The cross sections are in units of mb/(MeV sr^2). The bottom part of the figure shows the relative energies between each interacting pair.

two excited states $(1/2^-_1)$ and $(3/2^-_2)$, as represented in Fig. 4.

The spectroscopic factors, defined in Eq. (4), were obtained in the present paper as the ratio between the experimental values of Ref. [14] to the calculated values. The spectroscopic factors for each configuration are given in Table III. The figure shows that the optical potential parametrizations might change the detail of the momentum distribution at the maximum value and at the tail of the distribution. Nevertheless one can say that the Faddeev/AGS formalism is able to reproduce fairly well the available experimental data for p knockout with different interaction parametrizations. However, the deduced spectroscopic factors can vary significantly.

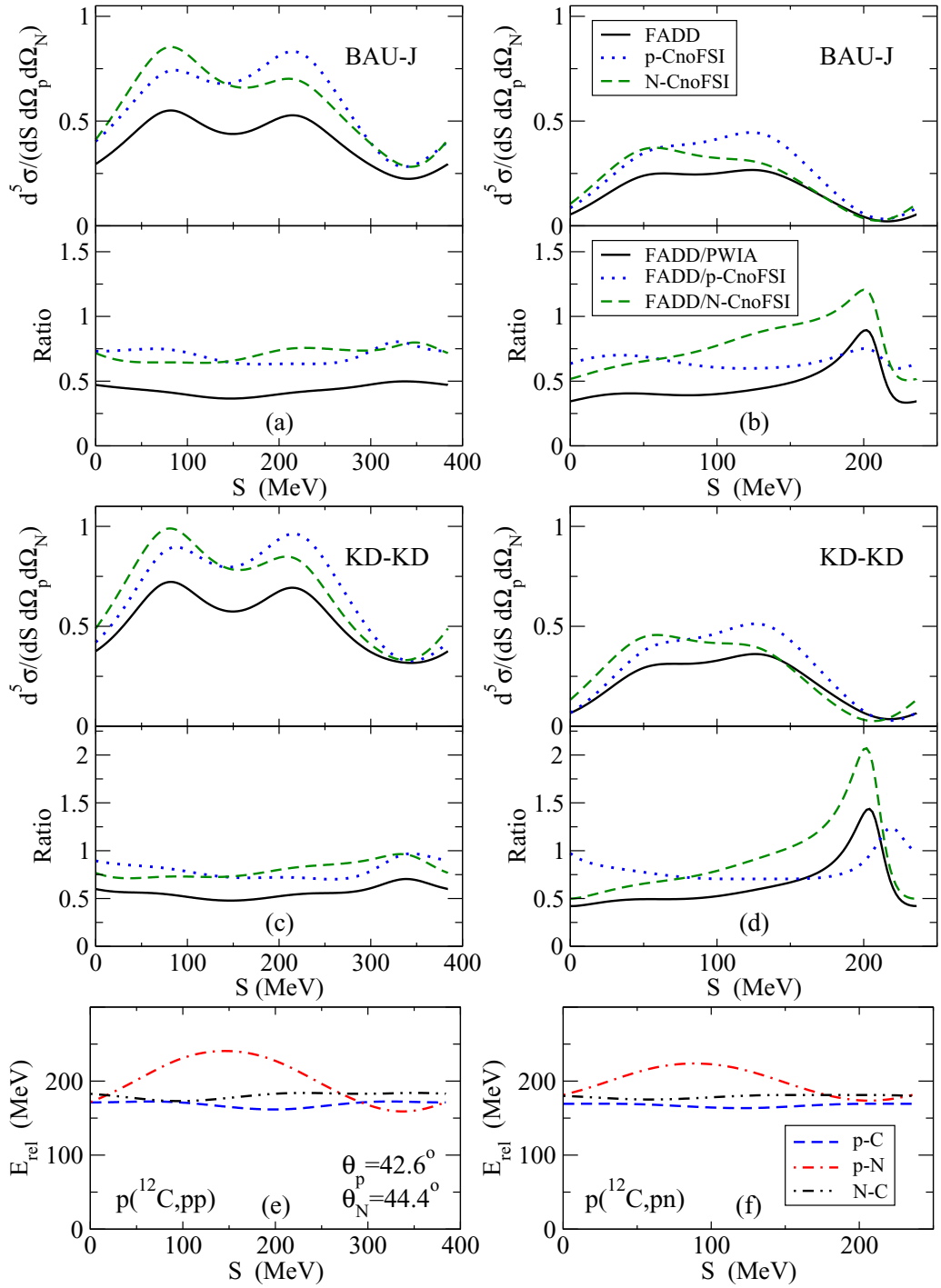

FIG. 17. The top and middle parts of the figure represents the kinematically fully exclusive cross sections as a function of the *S* parameter, $\frac{d^5\sigma}{dSd\Omega_p d\Omega_N}$, as defined in the text, for fixed polar angles and coplanar geometry, using two different optical potential parametrizations for *p* (left) and *n* (right) knockout. Also shown is the ratio between the FADD result and the PWIA approximation. The cross sections are in units of mb/(MeV sr^2). The bottom part of the figure shows the relative energies between each interacting pair.

VI. CONCLUSIONS AND OUTLOOK

We have studied (p, pN) reactions in inverse kinematics assuming a three-body description for the projectile and target system, and that the heavy fragment remains inert in the collision process.

We have used the exact Faddeev/AGS reaction framework that can be viewed as a multiple scattering expansion and have calculated three-body kinematically inclusive, semi-inclusive, and fully exclusive cross sections. We have shown that in the final state light particles are angle correlated with dominant coplanar kinematics, and the opening angle is close to the QFS

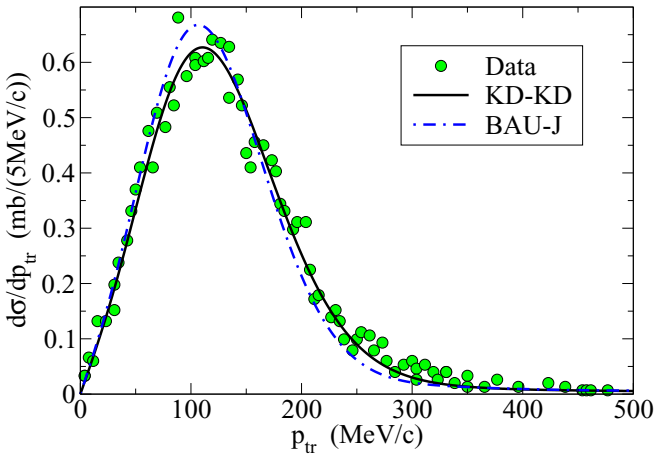

FIG. 18. Calculated heavy fragment (core) transverse momentum distribution $\sqrt{(p_x)^2+(p_y)^2}$ for the $p(^{12}\mathrm{C}, 2p)^{11}\mathrm{B}$ reaction leading to the ground state $(3/2^-_1)$ and the two excited states $(1/2^-_1)$ and $(3/2^-_2)$. The experimental data are taken from Ref. [14].

value of 90°; this indicates the dominance of the QFS reaction mechanism.

The twofold energy-angle and azimuthal-polar angle correlation cross sections and the angular correlation of the two light particles exhibit a distinct behavior for p and n knockout. In particular, while for p knockout the two light fragments are emitted preferably at 45°, for n knockout the neutron is emitted preferentially at 30°.

Several attenuating effects on the calculated PWIA were addressed. The kinematically fully exclusive differential cross sections show that the full and PWIA results are not related through a common integrated renormalization factor. For the case of proton knockout the renormalization remains close to the calculated integrated ratio while stronger deviations occur for the neutron knockout. Therefore, we can conclude that the approximate QFS amplitude (3) is valid for p knockout in some particular final-state kinematic configurations, but is more limited for the case of n knockout.

We have also found that the ratio of the full to no p-core FSI and no N-core FSI results is essentially constant for p knockout, but varies significantly for n knockout. Some configurations can be found where in some restricted kinematic phase space the deviation from a constant renormalization factor can be minimized. In general, this renormalization factor depends on the configuration, and deviates significantly from the integrated ratio.

Kinematically fully exclusive measurements of p and n knockout are needed in the future for the assessment of the role of distortions and FSI that is needed for a reliable understanding of projectile structure.

Finally we also show that the Faddeev/AGS formalism is able to reproduce fairly well the available experimental data for p knockout.

A similar study will be performed for other nuclei at/away from the stability line. The effects of introducing interactions derived from *ab initio* structure models need to be investigated as well as the effect of nuclear correlations not included in the current adopted choice of the Hilbert space for the projectile.

TABLE III. Calculated Faddeev/AGS total cross sections for p knockout and spectroscopic factors for the ground state $(3/2^-_1)$ and the two excited states $(1/2^-_1)$ and $(3/2^-_2)$ using the BAU-J and KD-KD optical potential parametrizations. The experimental data are taken from [14].

V	I^π_C	nlj	σ_{sp}(mb)	σ_{exp}(mb)	$\mathcal{Z}$
BAU-J	$3/2^-_1$	$1p3/2_1$	6.02	15.18(18)	2.52
	$1/2^-_1$	$1p1/2_1$	5.90	1.92(2)	0.33
	$3/2^-_2$	$1p3/2_1$	5.43	1.5(2)	0.28
					$\Sigma = 3.13$
KD-KD	$3/2^-_1$	$1p3/2_1$	8.54	15.18(18)	1.78
	$1/2^-_1$	$1p1/2_1$	8.50	1.92(2)	0.23
	$3/2^-_2$	$1p3/2_1$	7.90	1.5(2)	0.19
					$\Sigma = 2.20$

ACKNOWLEDGMENTS

The work of R.C. and E.C. was supported by Fundação para a Ciência e Tecnologia (FCT) of Portugal under Contract No. PTD/FIS-NUC/2240/2014. The work of A.D. was supported by the Alexander von Humboldt-Foundation under Grant No. LTU-1185721-HFST-E.

APPENDIX: FADDEEV/AGS EQUATIONS

The three-body Faddeev/AGS reaction approach is an exact nonrelativistic formalism where the transition amplitudes leading to the observables are the on-shell matrix elements of the operators $U^{\beta\alpha}$ obtained simultaneously for all open channels from the solution of the integral equations,

$$U^{\beta\alpha} = \bar{\delta}_{\beta\alpha} G_0^{-1} + \sum_\gamma \bar{\delta}_{\beta\gamma} t_\gamma G_0 U^{\gamma\alpha}, \tag{A1}$$

where $\bar{\delta}_{\beta\alpha} = 1 - \delta_{\beta\alpha}$, and

$$t_\gamma = v_\gamma + v_\gamma G_0 t_\gamma \tag{A2}$$

is the transition operator for each interacting pair. For example, v_1 denotes the interaction between the pair (2,3). The subscripts α, β, γ denote two-cluster configurations, i.e., the spectator particle or, equivalently, the pair in the odd-man-out notation. In Eq. (A2),

$$G_0 = (E + i0 - H_0)^{-1} \tag{A3}$$

is the free resolvent; E is total energy in the three-particle center-of-mass system. The $\beta = 0$ partition corresponds to three free particles in the continuum. The $\alpha = 1$ corresponds to the proton spectator in the incident channel.

The knockout amplitude, Eq. (A1), can be viewed as a multiple scattering expansion,

$$U^{\beta\alpha} = \bar{\delta}_{\beta\alpha} G_0^{-1} + \sum_\gamma \bar{\delta}_{\beta\gamma} t_\gamma \bar{\delta}_{\gamma\alpha} + \sum_\gamma \bar{\delta}_{\beta\gamma} t_\gamma \sum_\xi G_0 \bar{\delta}_{\gamma\xi} t_\xi \bar{\delta}_{\xi\alpha} + \cdots . \tag{A4}$$

The successive terms of this series can be grouped as terms of zero order (which contribute only for rearrangement transitions), first order (or single scattering term), second order (double scattering) in the transition operators t_γ, and so on.

The kinematic variables in the LAB system satisfy the law of conservation of momentum

$$\mathbf{K}_{\rm LAB} = \mathbf{K}_N + \mathbf{K}_p + \mathbf{K}_C, \tag{A5}$$

and energy

$$E_{\rm LAB} - \epsilon - \frac{K_N^2}{2m_N} - \frac{K_Z^2}{2m_Z} - \frac{(\mathbf{K}_{\rm LAB} - \mathbf{K}_N - \mathbf{K}_Z)^2}{2m_{\overline{Z}}} = 0, \tag{A6}$$

where $\mathbf{K}_{\rm LAB}$ is the beam momentum in the LAB frame, $E_{\rm LAB}$ is the corresponding energy, and ϵ is the separation energy of the knockout particle.

The kinematically fully exclusive fivefold differential breakup cross section is conveniently expressed in terms of the arc length S related to the LAB energies E_N and E_Z of the two detected particles as $S = \int_0^S dS$ [8] with

$$dS = \sqrt{dE_N^2 + dE_Z^2} = dE_Z \sqrt{1 + \left(\frac{m_Z K_N}{m_N K_Z}\frac{dK_N}{dK_Z}\right)^2} \tag{A7}$$

with

$$\frac{dK_N}{dK_Z} = -\frac{(m_{\overline{Z}} + m_Z)K_Z - m_Z(\mathbf{K}_{\rm LAB} - \mathbf{K}_N)\cdot\hat{\mathbf{K}}_Z}{(m_{\overline{Z}} + m_N)K_N - m_N(\mathbf{K}_{\rm LAB} - \mathbf{K}_Z)\cdot\hat{\mathbf{K}}_N}\frac{m_N}{m_Z}. \tag{A8}$$

[1] J. A. Tostevin and B. A. Brown, Phys. Rev. C **74**, 064604 (2006).
[2] A. Gade, R. V. F. Janssens, D. Bazin, R. Broda, B. A. Brown, C. M. Campbell, M. P. Carpenter, J. M. Cook, A. N. Deacon, D.-C. Dinca *et al.*, Phys. Rev. C **74**, 021302(R) (2006).
[3] E. C. Simpson, J. A. Tostevin, D. Bazin, B. A. Brown, and A. Gade, Phys. Rev. Lett. **102**, 132502 (2009).
[4] S. Soheyli and M. Khamehchi, Phys. Rev. C **82**, 014605 (2010).
[5] L. D. Faddeev, Zh. Eksp. Teor. Fiz. **39**, 1459 (1960).
[6] E. O. Alt, P. Grassberger, and W. Sandhas, Nucl. Phys. B **2**, 167 (1967).
[7] A. Deltuva, A. M. Moro, E. Cravo, F. M. Nunes, and A. C. Fonseca, Phys. Rev. C **76**, 064602 (2007).
[8] R. Crespo, A. Deltuva, M. Rodríguez-Gallardo, E. Cravo, and A. C. Fonseca, Phys. Rev. C **79**, 014609 (2009).
[9] E. Cravo, R. Crespo, and A. Deltuva, Phys. Rev. C **93**, 054612 (2016).
[10] R. Crespo, A. Deltuva, and E. Cravo, Phys. Rev. C **90**, 044606 (2014).
[11] N. Chant and P. Roos, Phys. Rev. C **15**, 57 (1977).
[12] R. Crespo, E. Cravo, A. Arriaga, R. Wiringa, A. Deltuva, and R. Diego, J. Phys.: Conf. Ser. **966**, 012056 (2018).
[13] L. V. Chulkov *et al.*, Nucl. Phys. A **759**, 43 (2005).
[14] V. Panin *et al.*, Phys. Lett. B **753**, 204 (2016).
[15] E. Cravo, R. Crespo, A. Deltuva, and A. C. Fonseca, Phys. Rev. C **79**, 064610 (2009).
[16] J. A. Lay, R. de Diego, R. Crespo, A. M. Moro, J. M. Arias, and R. C. Johnson, Phys. Rev. C **94**, 021602(R) (2016).
[17] M. Freer, H. Horiuchi, U.-G. M. Y. Kanada-En'yo, and D. Lee, Rev. Mod. Phys. **90**, 035004 (2018).
[18] R. Machleidt, Phys. Rev. C **63**, 024001 (2001).
[19] W. Bauhoff, Phys. Rev. C **31**, 253 (1985).
[20] K. W. Jones *et al.*, Phys. Rev. C **33**, 17 (1986).
[21] A. J. Koning and J. P. Delaroche, Nucl. Phys. A **713**, 231 (2003).
[22] E. C. Pinilla, P. Descouvemont, and D. Baye, Phys. Rev. C **85**, 054610 (2012).
[23] A. Deltuva, Phys. Rev. C **74**, 064001 (2006).